ЕКОЛОГІЯ

ECOLOGY

DOI 10.20535/1813-5420.4.2024.315598
M. Hajivand[1], PhD student, ORCID 0000-0002-9990-9761
D. Dolmatov[1], Dr. Sc. (Eng.), Assoc. Prof, ORCID 0000-0002-7268-1509
[1]National Aerospace University «Kharkiv Aviation Institute»

EFFECT OF LIQUID KEROSENE DROPLET INJECTION AT VARIOUS RADIAL AND TANGENTIAL VELOCITIES ON NOX, CO FORMATION, AND TEMPERATURE DISTRIBUTION

This research presents a numerical analysis and CFD simulation of liquid kerosene combustion by means of a variation of liquid kerosene radial and tangential velocity components of injected droplets through an atomizer into a real combustor. The droplets are considered through the Rosin-Rammler droplet particle size distribution with the Eulerian-Lagrangian Spray Atomization model. The main purpose of this investigation is to evaluate the behavior of emission formations such as NO and CO, including temperature distribution fluctuations in the primary combustion zone during the combustion process and droplet evaporation. For the simulation of evaporated kerosene combustion, the flamelet model was performed for the detailed kinetic scheme of chemical reactions between (JetA-C10H22) and air, which is integrated in ANSYS CFX, including the thermal and prompt prediction of NO. The standard k-ϵ turbulence model was used with enhanced wall treatment including P1 radiation model. Verification and validation of analysis results were considered in this study, where the results, such as temperature and NO formation in various radial distances of combustor, were compared with the real experimental results. The results showed that droplet behavior, influenced by injection velocities, significantly impacts the combustion process, including temperature distribution, NOx formation, and CO emissions especially in the primary combustion zone.

Keywords: *CFD, combustion, atomization, emissions, spray, droplet evaporation, flamelet.*

Introduction

In gas turbine engines the way that liquid fuel droplets are sprayed into the combustion chamber plays a role, in how the combustion process unfolds. The swirling movement of these droplets has an impact on factors like flame stability dynamics and overall structure. Understanding how liquid fuel droplets behave in swirling conditions specifically those made up of C10H22 (decane) is key to optimizing combustion efficiency and cutting down on harmful emissions such, as nitrogen oxides (NOx) and carbon monoxide (CO).

In gas turbine engines fuel atomization and droplet movement are engineered to generate a swirling turbulent flow that enhances the mixing of fuel and air, in combustion chambers. The centrifugal forces resulting from this swirl pattern produced by swirlers affect the distribution of fuel droplets in radial directions well, as tangentially in the injection process. The speed factors play a role, in influencing how heat is spread out and how flames move in the burning area while also affecting how long droplets stay there. One of the concerns in this scenario is the creation of NOx emissions which occur mainly at combustion temperatures due to the nitrogen and oxygen reaction, in the atmosphere. The duration of hot gas exposure and the temperature of the flame are factors, in NOX production process. Influenced by how swirling fuel droplets interact with the surrounding air environment. When fuel droplets swirl around it creates recirculation areas that alter the flames shape and can lead to varying levels of NOX and CO formation based on flow circumstances.

Researchers are working to create combustion systems that not only meet increasingly strict environmental laws but also ensure steady and efficient burning. Besides that, they are exploring the effects of swirling fuel droplets on flame dynamics and the formation of harmful substances produced in combustion products.

Even though studies on liquid fuel combustors have yielded a wealth of knowledge, more research should be done on the distribution of fuel injection output from fuel injection systems and the mixing process, which have a significant impact on the quantity and quality of pollutants released during combustion process [1].

Analysis of Recent Research and Publications

K. K. Rink and A. H. Lefebvre in 1989 [2], in their investigation reported that, atomization quality affects NO emission levels through the evaporation and mixing characteristics of the spray. Generally, the influence of

atomization quality is most apparent at slightly fuel-lean conditions, with reduced drop sizes leading to diminished NO, CO and UHC emissions.

Hajivand M et al. [1] showed in their study that atomization quality, such as the initial diameter of droplets and spray cone angle, affects emission levels through the evaporation and mixing characteristics of the spray; in other words, they improved that the influence of atomization quality is most definite at slightly fuel-lean conditions, with reduced initial drop sizes and cone angle of spray leading to decreased emissions.

The results of the investigation of Kankashvar et al. [3] showed that increasing the air flow rate decreased the stability range of the combustor, and increasing the fuel injection angle improved the lean blowout limit of the combustor and allowed it to work in extreme lean conditions. They also found that the temperature of the center of the chamber was lower with a higher fuel injection angle, and the temperature of the center of the chamber exit decreased with increasing air flow rate. Besides that, the authors concluded that increasing the spray cone angle improved the lean blowout limit of the chamber and allowed for flame stabilization even in extreme lean conditions.

The studies of Dafsari et al. [4] were aimed at the experimental analysis of atomization quality and the spray structure of aviation fuels with different viscosities, which were sprayed using a pressure swirl type nozzle with laser diagnostics. And they discovered that the injection pressure controlled both the overall spray structure and the quality of atomization of the fuel, which depended on the physical characteristics of the fuel. Lower viscosity fuels were found to be able to produce the ideal spray characteristics required in the combustion field, namely, well-developed hollow-conical sprays with finer drops, a wide distribution of size, and higher velocity components. It has been depicted that sufficient swirl intensity is necessary for the transitional development of hollow-conical sprays based on physical properties and injection pressure.

The decrease in pollutant emission concentrations for small droplet sizes is attributable to inadequate atomization with large droplet sizes, which causes localized fuel-rich burning, ultimately leading to the generation of soot and nitrogen oxides [4,5,6].

Bishop, K et al. [7] have investigated the impact of fuel nozzle condition on temperature distributions in nozzle guide vanes using an optical patternator. Their study quantified average spray cone angle, symmetry, and fuel streaks. Besides that, an ambient pressure and temperature combustion chamber test rig was used to capture exit temperature distributions and determine the pattern factor. Their obtained results showed that small deviations from the nominal distribution in the fuel nozzle spray pattern led to an increased pattern factor, possibly due to degradation of mixing processes. Spray cone angle had the most significant influence, while spray roundness and streak intensity had less influence. Comparisons were made with published studies on combustion chamber geometry, and recommendations for fuel nozzle inspections were made.

Many researchers conducted experimental studies on fuel spray atomization and employed CFD methodologies, concluding that the atomizing gas significantly influences spray atomization [3,8,9,10].

The spray angle, derived from high-quality pictures, significantly affects both the spray pattern and droplet size [11]. Gong and Fu [12] examined the impact of structural factors and viscosity on the spray angle of a swirling atomizer employed in combustion. They utilized oil in their studies and established empirical correlations to ascertain the discharge coefficient and spray angle.

The purpose of this study

During the CFD study conducted here were six scenarios analyzed to delve into how changing velocity components in different kerosene injection directions, such as radial and tangential, impacts combustion dynamics and flame characteristics while affecting the levels of NOx, CO emissions, and temperature distribution, implemented in ANSYS CFX [15,16].

The initial three cases concentrated on examining the changes in tangential velocity of droplets injected into the combustion chamber. Besides that, the other cases were the variation of the droplet radial injection velocity. The main goal in these scenarios was to assess the performance of the combustion procedure in the area where maximum NOx development happens. This region is distinguished by temperatures and strong chemical responses, making it essential to comprehend how the spinning droplets impact the flame front and general combustion dynamics. The appearance of the flame and how steady and strong it combusts are factors in gauging how well combustion is working and what emissions are being produced. Our goal was to study how adjusting the swirling radial and tangential velocity affects these characteristics, specifically focusing the creation of CO, NOx, and temperature distributions in the primary combustion zone.

The main material of the study

The governing equations, turbulence, mathematical modeling of combustion process and radiation

The principles, behind fuel combustion are built upon rules related to preservation and the transfer of momentum and energy in addition to incorporating extra equations to address turbulence and combustion mechanisms. The research employs the known k–ε turbulence model which tackles two equations – one for the turbulent kinetic energy (referred to as k) and the other, for how this energy dissipates (indicated as ε). Through the years turbulence models have been crafted by scientists offering levels of intricacy and applicability across different scenarios. In this study approach, to modeling turbulence properties for high Reynolds numbers in flows

involves solving two differential equations – one for kinetic energy (referred to as k) and another for dissipation rate (referred to as ε). Although this method is moderately intricate in nature it has garnered acceptance in research works due to its effectiveness, under diverse flow scenarios. The initial equations that form the basis of this model were initially presented by Launder and Spalding in 1974.

The constant model of PDF (Probability Density Function) flames created by Peters [13] relies on ideas; It suggests that turbulent combustion happens through multiple separate and stable laminar flames and that the flames thickness is less, than the smallest turbulent length scale (referred to as the Kolmogorov length scale) enabling the flame structure to stay laminar [14]. The turnover time, for eddies is longer than that for chemical reactions in this context; hence any short-lived effects are considered insignificant within the model's framework. Furthermore, this model has been incorporated into CFD software such as Fluent, Star. CD, Star. CCM and CFX. Its widespread usage, across applications can be attributed to its effectiveness strong convergence capabilities and satisfactory level of accuracy [14]. In this study Jet-A aviation fuel (kerosene) with air, modeled as a two-component surrogate fuel (by mass 60 % C10H22 and 40 % C9H12).

In the laminar flamelet model available in ANSYS CFX, the species mean mass fractions are stored in the flamelet library as a function of the mean mixture fractions $\tilde{Z}$, its variance $\widetilde{Z''^2}$ [16,]. The Favre mean species mass fraction can then be calculated with a probability density function $\tilde{P}$ [16,17].

$$\tilde{Y}_i = \int_0^1 Y_i(Z, \tilde{\chi}_{st})\tilde{P}(Z)dZ \tag{1}$$

typically, a β-function is used as the pdf of the mixture fraction is used, which in other words, it can be written like $\widetilde{P}(Z, x, t)$. The pre-integration of flamelet tables is done with CFX-RIF [16] automatically.

In the flamelet model context of solving transport equations, for each chemical element we focus solely on the transport equations for the Favre average mixture fraction and its variance. By assuming rates for all species (uniform diffusivities) we can represent the transport equation, for the Favre mean mixture fraction as;

$$\frac{\partial(\bar{\rho}\tilde{Z})}{\partial t} + \frac{\partial\left(\bar{\rho}\tilde{u}_j\tilde{Z}\right)}{\partial x_j} = \frac{\partial}{\partial x_j}\left[\left(\bar{\mu} + \frac{\mu_t}{\sigma_Z}\right)\frac{\partial\tilde{Z}}{\partial x_j}\right] \tag{2}$$

Where μ is the molecular dynamic viscosity, μ_t the turbulent viscosity and σ_Z is a model coefficient. As the mixture fraction is a conserved scalar, its transport equation contains no source term. The transport equation for the mixture fraction variance $\widetilde{Z''^2}$ can be modeled as follows [16].

$$\frac{\partial\left(\bar{\rho}\widetilde{Z''^2}\right)}{\partial t} + \frac{\partial\left(\bar{\rho}\tilde{u}_j\widetilde{Z''^2}\right)}{\partial x_j} = \frac{\partial}{\partial x_j}\left[\left(\bar{\mu} + \frac{\mu_t}{\sigma_{\widetilde{Z''^2}}}\right)\frac{\partial\widetilde{Z''^2}}{\partial x_j}\right] + 2\frac{\mu_t}{\partial_Z}\left(\frac{\partial\tilde{Z}}{\partial x_j}\right)^2 - \bar{\rho}\tilde{\chi} \tag{3}$$

where $\sigma_{\widetilde{Z''^2}}$ and $C\chi$ in equation (4) are model coefficients. The first term on the right-hand side represents the production of variance, whereas the last term models its dissipation. The instantaneous scalar dissipation rate is modeled as [16].

$$\tilde{\chi} = C_\chi\frac{\tilde{\varepsilon}}{\tilde{k}}\widetilde{Z''^2} \tag{4}$$

With $\tilde{\varepsilon}$ and $\tilde{k}$ being the dissipation rate and the turbulent kinetic energy, respectively. As the species mass fractions are previously stored in a flamelet table, they can be obtained within the CFD simulation by coupling the CFD code with the flamelet libraries [13].

In the flamelet concept framework of combustion modeling the characteristics of the Favre mixture fraction. Its variation, alongside the scalar dissipation rate are calculated utilizing computational fluid dynamics (CFD). These quantities are subsequently employed to extract already computed species mass fractions, from a library dedicated to flamelet models [18].

Heat transfer plays a role, in fine-tuning and testing combustion system layouts with radiation being an element involved. In the context of a combustion system heat transfer takes place through conduction, radiation and inter diffusion [19]. Combustion essentially involves oxidation that produces heat and radiation underscoring the importance of radiation, in the chemical reaction process. At temperatures thermal radiation emerges as a means of energy transfer and needs to be taken into account when implementing a practical combustion system [19].

While radiation itself doesn't have an impact, on reactions, it does play a role in influencing the distribution of flame temperatures, which then affects various aspects of combustion processes. In research conducted by Chan and Viskanta back, in 2005 it was demonstrated that radiation can significantly alter flame temperatures, the concentrations of minor species present NOx emissions levels, soot generation tendencies, flame extinguishment behavior and other phenomena related to combustion. The Differential Approximation (known as the P1 model) offers a method, for tackling the radiation transport equation by assuming that radiation intensity is uniform in all directions at a point, in space. A comprehensive explanation of the energy equation and the development of the P Model 2 are detailed by Modest [16,20].

Discrete particles numerical modeling

In the ANSYS CFX Theory Guide [16] when it comes to particle numerical modeling and simulating fluid movement using the Euler method specifically, the communication between various phases is depicted using distinct physical models [21]. The movement of mass between these phases is mimicked using a model for evaporation in this scenario. ANSYS CFX employs the Antoine equation (Equation 5) to replicate this process by determining the boiling point of kerosene [21]. The equation helps us establish the boiling point, which is then utilized to specify the source term for mass transfer in the simulation.

$$p_{\text{var}} = p_{\text{scale}} \cdot \exp\left(A - \frac{B}{T_p + C}\right) \tag{5}$$

In this case, T_p denotes the temperature of the droplet, while p_{scale} stands for a scaling factor; A, B, and C represent factors derived from reputable sources as, per this investigation, data about kerosene (C10H22). Studies indicate that slight alterations in the values of A, B, and C—falling within the range for hydrocarbons to kerosene—lead to negligible impacts in combustion efficiency, with an error margin of under 1.5%.

Using the size droplets uniformly spread out in the coolant liquid application process recommended a Rosin Rammler distribution, for better simulation accuracy without major changes to key parameters [22]. The Rosin Rammler model defined in (Equation 6) is frequently utilized in contemporary spray combustion simulations due to its effectiveness and efficiency. Has been implemented in both core flow and coolant injection scenarios, for this investigation [22]. In this chapter, we have talked about the Rosin Rammler distribution before. Now it's being shown in a light.

$$f(d) = \frac{q}{D}\left(\frac{d}{D}\right)^{q-1} \cdot \exp\left[-\left(\frac{d}{D}\right)^{q}\right] \tag{6}$$

where D is the size parameter, q for spread parameter and d stand for droplet diameter [16].

During the phase of dispersion analysis is conducted to establish the source terms between phases as outlined in the gas phase conservation equations. The spray is depicted as consisting of droplet categories spread out over an initial dispersion range. The speed, distance, mass and temperature of each category are monitored over time along their trajectories by applying the conservation equations within a Lagrangian framework [23].

This method enables monitoring of how everything behaves when it interacts with the fluid around it.

In the kth category we figure out how a moves, by looking at its speed and location along the way using a droplet as a reference point. The droplet speed is calculated based on the balance of forces. Considering both the droplets inertia and the drag force that affects it. This equation, for momentum can be expressed as follows:

$$m_d(k)\frac{du_{d_i}(k)}{dt} = \frac{\pi}{8}\tilde{\rho}[d(k)]^2\left|u_i - u_{d_i}(k)\right|\left[u_i - u_{d_i}(k)\right]C_{drag} \tag{7}$$

The drag coefficient, C_{drag} ,is evaluated following the spherical drag low [23].

The process of evaporation, from the droplets surface is simulated by assuming that the vapor pressure on the droplets surface matches the saturation pressure at the droplet's temperature [23]. To figure this out accurately for the liquid fuel used in this scenario a linear relationship between saturation pressure and temperature is applied in sections. The mass transfer coefficient is determined by referencing the Sherwood number correlation from Ranz and Marshall [24]. Consequently, we can represent the change in mass caused by evaporation, with:

$$\frac{dm_p}{dt} = \pi d_p^2 h_D\left(C_{fs} - C_f\right) \tag{8}$$

Where C_{fs} and C_f are the mass fractions of the fuel vapor on droplet surface and in the surrounding gas.

When determining how the temperature of a changes as it travels along its path, we apply an energy balance across the surface of the droplet. This balance considers both the heat transferred to the droplet through convection and the latent heat needed for evaporation. It can be written out in this way:

$$m_P c_{p_p}\frac{dT_P}{dt} = hA_P(T - T_P) - \frac{dm_P}{dt}\Delta H_V \tag{9}$$

The heat transfer coefficient (h) is calculated using the Nusselt number correlation from Ranz and Marshall [24], with radiation exchange with the gas phase being neglected.

NOx formation modeling

In gas flames that reach temperatures exceeding 1800 Kelvin (1527 degrees Celsius), the primary source of nitrogen oxide (NOx) is the presence of nitrogen and oxygen radicals in the environment within the flames grasp. The creation of NO or Zeldovich NO in conditions follows a sequence of simple chemical reactions as explained by Zeldovich in 1946 and elaborated upon by Baulch and others in 1994 [25]. Nitric oxide (NO) is a component formed when oxygen and nitrogen radicals interact with each other under elevated temperature circumstances. The Zeldovich mechanism involves two steps. Is accountable for reactions (denoted as R1 and R2). [16]. When the air fuel ratio leans towards either stoichiometric level, in certain scenarios a third reaction (referred to as R3) could start playing a significant role in the process alongside the initial two reactions. This phenomenon is known as the Zeldovich mechanism. The term "thermal" is employed because the first reaction requires a high activation energy owing to the bond found in N2 molecules. This characteristic causes the reaction to occur swiftly

at temperatures [25]. The initial response serves as the step that controls the speed at which thermal NO is generated in production processes. The speeds associated with each reaction (R1, R2, R3) are listed following their reactions.

$$O + N_2 \overset{k_1}{\rightarrow} NO + N \qquad so \rightarrow \qquad k_1 = (1.8 \cdot 10^{11})\exp\left(-\frac{38370}{T}\right) \tag{R 1}$$

$$N + O_2 \overset{k_2}{\rightarrow} NO + O \qquad so \rightarrow \qquad k_2 = (6.4 \cdot 10^{9})\exp\left(-\frac{3162}{T}\right) \tag{R 2}$$

$$N + O_2 \overset{k_3}{\rightarrow} NO + O \qquad so \rightarrow \qquad k_3 = 3.0 \cdot 10^{3} \tag{R 3}$$

When multiply the rates of reaction, by the concentrations of the substances involved in the reaction process and express it in [kmol/m³/s] it can then convert this outcome into a mass source term. This term indicates how much mass is being produced or used up, per unit volume within the system.

$$\frac{d[NO]}{dt} = k_1[O][N_2] + k_2[N][O_2] + k_3[N][OH] \tag{10}$$

So:

$$\frac{d[NO]}{dt} = k_1[O][N_2] - k_2[N][O_2] - k_3[N][OH] \tag{11}$$

In ANSYS CFX Solver Theory Guide [16], the thermal formation in, $\mathrm{kg/m^3/s}, S_{NO,\,\mathrm{thermal}}$,as described is therefore related to the rate of Reaction (R1):

$$S_{\mathrm{No,thermal}} = 2W_{\mathrm{No}}\, k_{\mathrm{thermal}}\, [O][N_2] k_{\mathrm{thermal}} = k_1 \tag{12}$$

This denotes the molecular mass of NO. Therefore, if the molar concentrations [O] and [N2] of O radicals and N2 are established, the thermal NO mechanism can be assessed [16].

Prompt NO formation happens when temperatures drop below 1800 K and since our simulation is conducted at temperatures exceeding 2000 K, we won't delve into the details of how NO forms but will incorporate the thermal formation of NO into the simulation.

In the process of conducting a CFD simulation we address the mass transport equation concerning the NO species by considering factors, like convection, diffusion, NO generation and consumption alongside species. This approach is essentially rooted in the concept of preserving mass. To accurately represent prompt reactions, we rely on the transport equation specific, to the NO species mentioned earlier [26].

$$\rho \frac{\partial Y_{NO}}{\partial t} + \rho u_i \frac{\partial Y_{NO}}{\partial x_i} = \frac{\partial}{\partial x_i}\left(\rho D \frac{\partial Y_{NO}}{\partial x_i}\right) + S_{NO} \tag{13}$$

The source term S_{NO} is to be determined for different NOx formation mechanism.

Validation of the employed combustion CFD model

With all the studies done about combustion systems so far, researchers have noticed a big gap when it comes to experiments specifically looking at how liquid fuels burn in combustion chambers. Many of the studies don't dive deep into measuring emissions, like NOx levels and the amounts of important compounds, at the outlet of the combustor. Engineers and researchers usually hold back from sharing results in these areas, especially when it comes to how the related processes work in real-life situations and the complex behavior of jet stabilized configurations using liquid fuel. The limited availability of published findings underscores the obstacles and the necessity, for empirical research to comprehensively grasp the intricate interplays that influence NOX emissions and other crucial performance factors, in these systems.

Recent research has thoroughly investigated the combustion and nitrogen oxide emission properties of jet-stabilized combustors. In a jet-stabilized combustor type, secondary air is injected by four radial wall jets, essential for flame stabilization [27]. This arrangement is non-swirling and does not depend on swirl-induced stabilization, in contrast to standard setups. Consequently, jet stabilization provides an extensive operational range, rendering it especially appealing for both experimental and numerical investigations (Bauer et al., 2020) [28].

In their study [28], Bauer and his team conducted experiments to understand how combustion and NOx emissions occur in a jet-stabilized combustor. Kurreck and colleagues [29] used the k-epsilon turbulence model to forecast how flow patterns and temperature are distributed inside the combustor. In a study conducted by Bazdidi Tehrani and Zeinivand [30, 31], they used a method that combined the realizable k-epsilon turbulence model with presumed probability density functions (PDF) to replicate spray combustion in a jet-stabilized configuration. Their investigation also looked into how changing the quantity and locations of stabilizing jets affects both the efficiency of combustion and the emissions of NOx. The findings suggested that extending the distance of the stabilizer jets lowers NO emissions while increasing the number of jet orifices results in NO emissions.

In addition, to that point mentioned above by Bazdidi Tehrani and Teymoori [32], they worked on improving the jet stabilized combustor to reduce the emission of substances like NOx and soot particles. Their goal was to enhance this optimization process by adjusting the properties of the combustion chamber such as diameter, angle, and positioning of the stabilizing air jets. Their study also discusses the application of modeling

approaches like simulations, artificial neural networks, genetic algorithms, and multi-criteria decision-making techniques to reach optimal results. Furthermore, the article outlines the optimization process steps, the specifics of the simulations used, and validates these simulations by comparing them to data.

A study conducted by Alemi and colleagues [33] explored the impact of adjusting the angle and diameter of jet injection on NO emissions optimization results. The results were noteworthy; higher jet Reynolds numbers indicate an influence of injection angle on minimizing NO emissions at a 20° downstream angle. These findings underscore the importance of jet configuration for emissions control and improving the efficiency of jet-stabilized combustors.

The schematic of jet-stabilized combustor, mesh and boundary condition for investigation validation

The geometry of the present model combustor is inspired by the experimental setup documented by Bauer et al. [28]. As shown in (Fig. 1 a.).

The combustor is 400 millimeters long and 80 millimeters, in diameter with four stabilizing air jet holes measuring 8 millimeters each in diameter. These holes are placed around the circumference at intervals of 90 degrees. Are situated 60 millimeters away from the inlet plate. Moreover, a central liquid fuel atomizer of the air blast type (as seen in Fig. 1.) is installed in the combustor to ensure blending of fuel and air. The atomizer sprays fuel through a nozzle that's 0.7 mm of diameter, while air is discharged around the nozzle in a disk pattern with an inner diameter of 1 mm and an outer diameter of 3 mm [28]. To ensure accurate simulation of the turbulent flow within the model combustor, the computational domain is discretized using a structured mesh with 1,545,397 elements that includes a boundary layer, as shown in Fig. 1 a and b, employing the ICEM-CFD software generates multi-block structured meshes of the combustors.

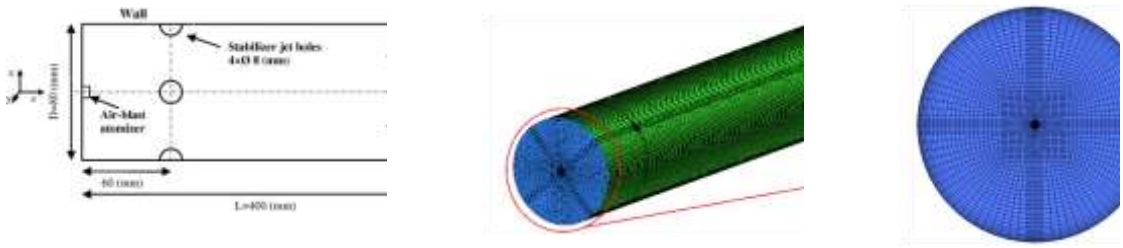

a) b) c)

Figure 1 – *The schematic and mesh of combustor a) Geometrical parameters; b) General view of combustor structured mesh c) The view of structured mesh with O-grid at center of injector*

The boundary conditions are in atmospheric pressure with 1 atm [28] and 295K of temperature, the air mass flow of atomizer is 0.00033 kg/s, air mass flow through the jets is 0.0093 (kg/s) and liquid fuel ($C_{10}H_{22}$) mass flow rate is 0.00028 kg/s. For the modeling of droplet distribution Rosin-Rammler droplet size is 20 (micron) with the power of 2.5 and the initial droplet velocity is 10.5 m/s.

The simulation of combustion of kerosene in gas form was implemented in flamelet model of combustion and the combination of finite rate chemistry and eddy dissipation model FRC/EDM [16].

The NOx formation and temperature distribution

As shown in Figures 2a and 2b, the temperature distributions at Z=1.75D and Z=2.275 demonstrate that the deviation between the CFD results, using the flamelet and FRC/EDM models, is not significant, which means less than 10%. Additionally, the comparison between the CFD results and the experimental temperature distribution obtained by Bauer et al. [28] at the same distances (mentioned above) shows good agreement, further validating the accuracy of the simulation.

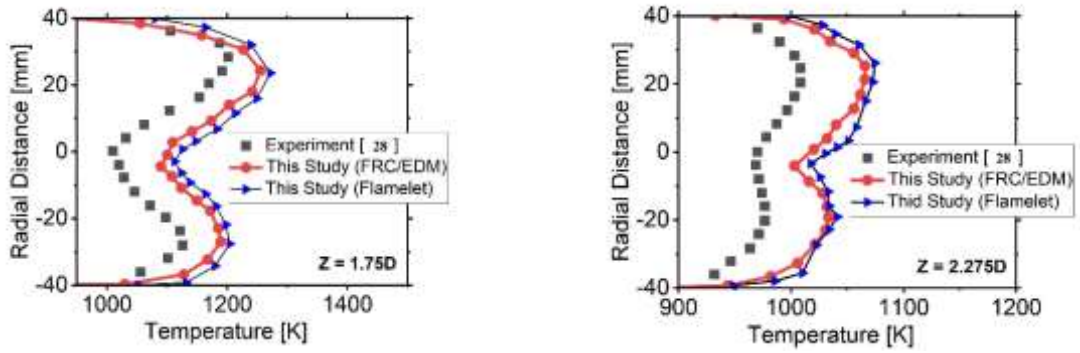

a) b)

Figure 2 – *Temperature distribution; a) in Z = 1.75D b) In Z = 2.275D*

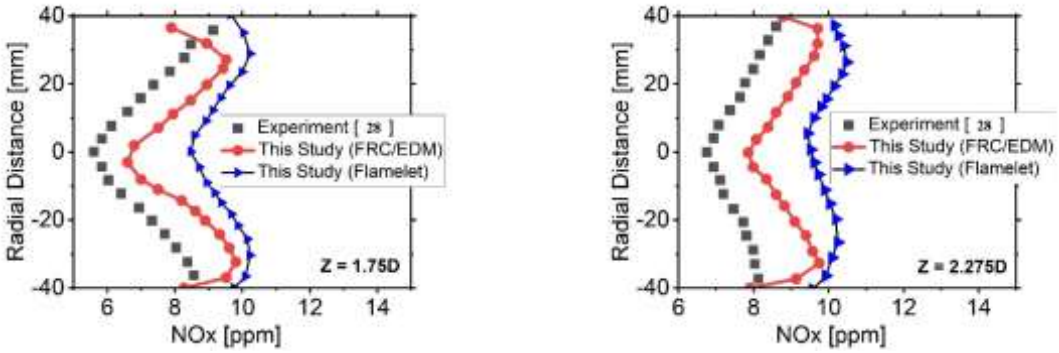

a) b)

Figure 3 – *The NO distribution; a) In Z = 1.75D b) In Z = 2.275D*

Figures 3a and 3b illustrate that at a distance of Z=1.75D, the discrepancy between the NO distribution forecasted by the flamelet model and the experimental results from Bauer et al. [28] surpasses 20%. At Z=2.275, the discrepancy between the flamelet model and the experimental results diminishes, indicating enhanced concordance. The NO concentrations predicted by the flamelet model significantly diverge from the experimental data, unlike the temperature outcomes, suggesting a substantial inconsistency that necessitates additional examination. This discrepancy indicates that further parameters, such as model assumptions or NO generation mechanisms, should be evaluated to enhance the simulation's accuracy.

The findings derived from the FRC/EDM model demonstrate a robust correlation with the experimental data at both distances, signifying enhanced predicted accuracy for NO distribution.

The main investigated combustor, combustion mathematical model, mesh and boundary conditions

The CFD study was conducted using a CAN combustion chamber that was previously introduced in studies by Prakash Ghose et al [23, 34, 35]. The combustion chamber is depicted more in Fig. 4a. The simulation was carried out in the same conditions that were explained in the abstract.

However, for a clearer examination of the development of the flame front and the formation of nitrogen oxides (NOx), including temperature and CO distribution, we adjusted the conditions for this study in a way that differs from what was presented in Ghose Prakash et al. research. Specifically, we made changes to the mass flow rates for both the fuel and air streams to gain an insight into NOx formation within a rich combustion setting.

The rate at which secondary air entered the combustion chamber was lowered to 0.005 kg/s to minimize its impact on the combustion process. This enabled us to examine the dynamics of the burn flame without being diluted by the air. Besides that, the flow rate of swirling air was changed to 0.05 kg/s. The C10H22 fuel flow rate was adjusted to 0.001 kg/s. By adjusting these factors, our goal is to offer an understanding of how the mixing of fuel and air caused by swirl affects the creation of flames and the release of NOx emissions, addressing the gaps that exist due to the constraints of experiments.

In Fig. 4b, the velocity distribution within the combustion chamber is shown under cold flow conditions (without combustion). The study utilized flow streamlines to anticipate the recirculation zone and internal velocity distribution crucial for setting and determining the axial injection velocity in our experiments. The cold flow simulation enabled us to concentrate on flow behaviors and notably the development of the recirculation zone.

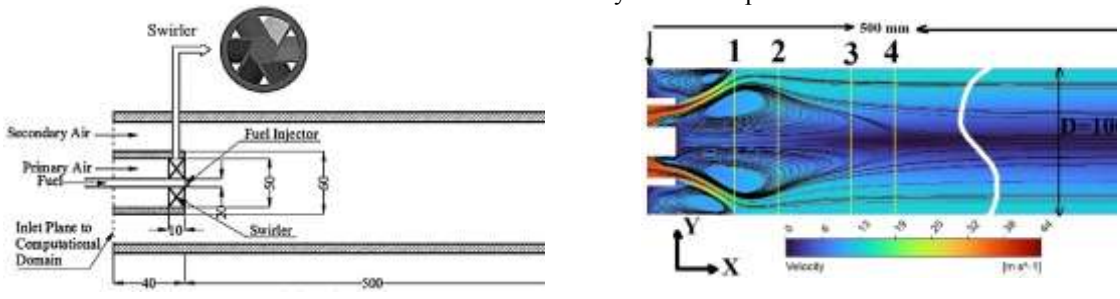

a) b)

Figure 4 – *The geometry and area of simulation; a) Physical geometry of the real combustor under study (Ghose P. et al.) [23,34,35]. b) The cold flow simulation contour plot of velocity and the area of investigation 1) X=0.04m 2) X=0.07m 3) X=0.0.12m 4) X=0.15m*

Also, in Fig. 4b, the illustration indicated that the velocity near the fuel atomizer falls within the range of 30 to 35 meters per second (m/s). In order to maintain a flame formation and prevent any instabilities from arising, we settled upon an axial injection speed of 30 m/s for all scenarios under examination. This choice was influenced

by the necessity to restrict the injection velocity so it does not surpass the velocity around the atomizer and, within the CRZ zone, since surpasses could disturb flame structure and result in combustion instabilities. Matching the velocity of the injection with how the flow behaves in a cold flow situation ensures that the burning process stays steady and controlled when faced with real combustion conditions.

The cases of study

In this investigation, six different cases were examined, as outlined in Table 1. These cases were designed to explore the effects of varying droplet radial and tangential velocities on combustion dynamics, temperature distribution, flame behavior, NOx and CO formation in the primary zone of combustion.

Table 1 – The various of atomization injection velocity component in various cases.

Cases	Axial velocity (m/s)	Radial velocity (m/s)	Tangential velocity (m/s)
1th Case	30	0	10
2th Case	30	0	17
3th Case	30	0	30
4th Case	30	5	17
5th Case	30	12	17
6th Case	30	27	17

The research, in the first three cases, delved into evaluating the changes in tangential velocity of C10H22 droplets inside the combustor. The main objective in these scenarios was to investigate how the combustion process behaves in the region where NOx generation and temperature distribution are at their peak. The primary zone of combustion is noted for its high temperatures and powerful chemical reactions that underline the necessity of knowing how spinning droplets effect the flame properties, emission generation, and overall combustion dynamics.

In contrast to that, the fourth, fifth, and sixth cases investigated how the radial injection velocity of C10H22 droplets impacts the combustion process and emission formation in the primary zone of combustion. In other words, we investigated in these 3 cases how liquid fuel droplets are distributed within the combustor and affect mixing efficiency and flame characteristics, including the formation of NOx and CO.

Results and discussion for the Temperature distribution, NOx and CO formation

Fig. 5 a. (Temperature distribution at X = 0.04 m): The temperature distribution in the combustor's primary zone varies noticeably between the six scenarios. Due to less effective combustion and weaker fuel-air mixing, the first example has the lowest temperature (1377K). The temperature increases dramatically in the later cases, especially in the third and sixth examples, as the tangential and radial velocities grow. In the sixth case, the temperature reaches 1808K. Higher velocities boost mixing, which encourages more thorough burning and produces a hotter flame in the primary zone's core, which is the reason for this rise. The second, fourth, and fifth intermediate examples exhibit temperatures ranging from 1576K to 1656K, demonstrating the rising effect of higher droplet velocities.

Fig. 5 b. (Temperature distribution at X = 0.07 m): At this axial location, there are still noticeable changes in the flame core temperature, but the distribution of temperatures along the combustor wall becomes more consistent. The maximum core temperature in the first case is 1815K, and the highest temperature in the sixth case is 1960K. The core temperature indicates the strength of the combustion process, while the homogeneity around the walls is a sign of stable heat transport. Better fuel-air mixing and greater flame temperatures in the core are the results of the later cases' higher tangential and radial velocities, particularly in the third and sixth examples.

Fig. 5 c. (Temperature distribution at X = 0.12 m): As the flow progresses, the temperature differences between the six cases diminish. The fluctuation is minimal, with temperatures ranging from 1985K in the first case to 2010K in the third and sixth cases. This indicates that the combustion process has largely stabilized, with the flame maintaining a high and consistent temperature. The reduced variation suggests that the fuel has been mostly consumed, and the combustion process is nearing completion.

Fig. 5 d. (Temperature distribution at X = 0.15 m): By this axial position, the temperature fluctuations among the cases remain minimal, as in Fig. 5 c. The temperatures range from 1978K in the third case to 2005K in the first and sixth cases. This consistency reflects the complete combustion occurring by this point, where the fuel is almost fully oxidized, and the temperature stabilizes throughout the chamber.

Fig. 6 a. (NO distribution at X = 0.04 m): The NO distribution at the primary zone of combustion corresponds to the temperature fluctuations illustrated in Fig. 5a. The first case has the lowest NO concentration (8.43 ppm), which correlates with its reduced flame temperature. With the increase in tangential and radial velocities in the successive cases, NO production escalates markedly, culminating in the sixth scenario at 26.24 ppm. This is because NO generation, particularly thermal NOx, is extremely temperature-dependent, and the higher temperatures in the later situations promote more NO formation in the flame core.

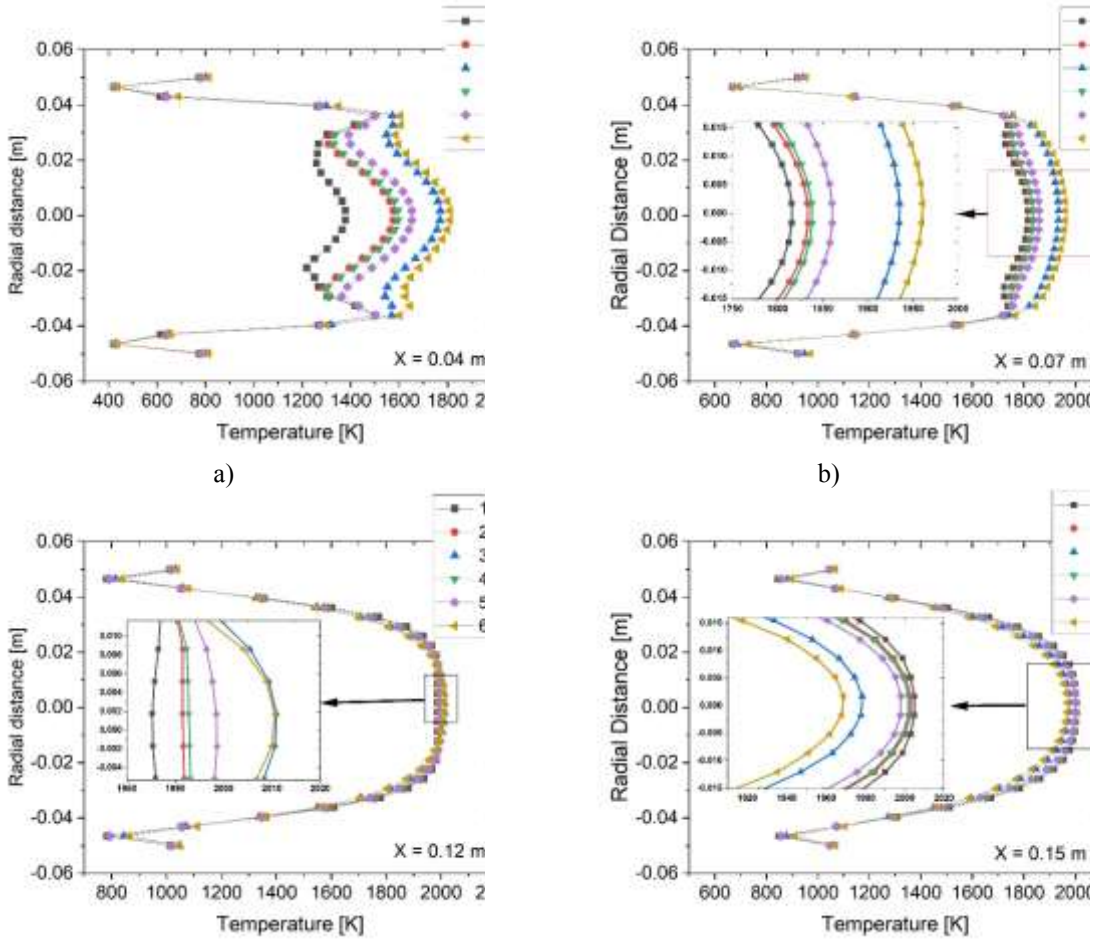

Figure 5 – *Temperature distribution in various location of the combustor for various cases*

Fig. 6 b. (NO distribution at X = 0.07 m): At this point, NO formation increases substantially compared to X = 0.04 m. The first case has a maximum NO concentration of 13.67 ppm, while the sixth case peaks at 39.71 ppm. The increase in NO is driven by the higher temperatures at this axial position, as shown in Fig. 5 b, and the prolonged exposure of the flame to high temperatures. The third and sixth cases, which have the highest flame temperatures, naturally produce the most NO.

Fig. 6 c. (NO distribution at X = 0.12 m): By X = 0.12 m, the NO levels continue to rise, with the sixth case reaching a peak of 67.7 ppm, while the first case remains at 37.8 ppm. The increased NO formation is a result of sustained high temperatures in this region, as indicated by the temperature distribution in Fig. 5 c. The next cases, with their higher initial droplet velocities and better fuel-air mixing, produce more NO due to the extended time the flame spends at elevated temperatures.

Fig. 6 d. (NO distribution at X = 0.15 m): At the last location, the NO level remains high, with the first case at 56.84 ppm and the sixth case at 67 ppm. The slight drop in NO from X = 0.12 m to X = 0.15 m in some cases suggests that NO formation has slowed as the combustion process nears completion. However, the high NO concentrations across all cases reflect the sustained high temperatures in the flame core, as seen in Fig. 5 d.

Fig. 7 a. (CO distribution at X = 0.04 m): According to the CO distribution, the greatest mass fraction in the first, second, and third examples is 0.086, 0.089, and 0.087, respectively, resulting in quite high CO concentrations in the flame core. The greater CO in these circumstances is a symptom of incomplete combustion, where insufficient oxygen hinders the entire oxidation of carbon to CO2. The fourth, fifth, and sixth examples show a minor decrease in CO mass fractions as the radial velocity increases; the sixth case, in particular, reaches a minimum of 0.085, indicating more efficient burning and less CO generation.

Fig. 7 b. (CO distribution at X = 0.07 m): CO concentrations start to decrease as burning continues. The CO mass fraction in the first case is still somewhat high at 0.098, but it is lower in the third and sixth cases at 0.077 and 0.069, respectively. The higher temperatures in Fig. 5 b, are indicative of enhanced combustion efficiency at this axial point, which is responsible for the decrease in CO. The greater droplet velocities appear to facilitate more thorough combustion, generating more CO2 from CO, as evidenced by the lower CO levels in the latter examples.

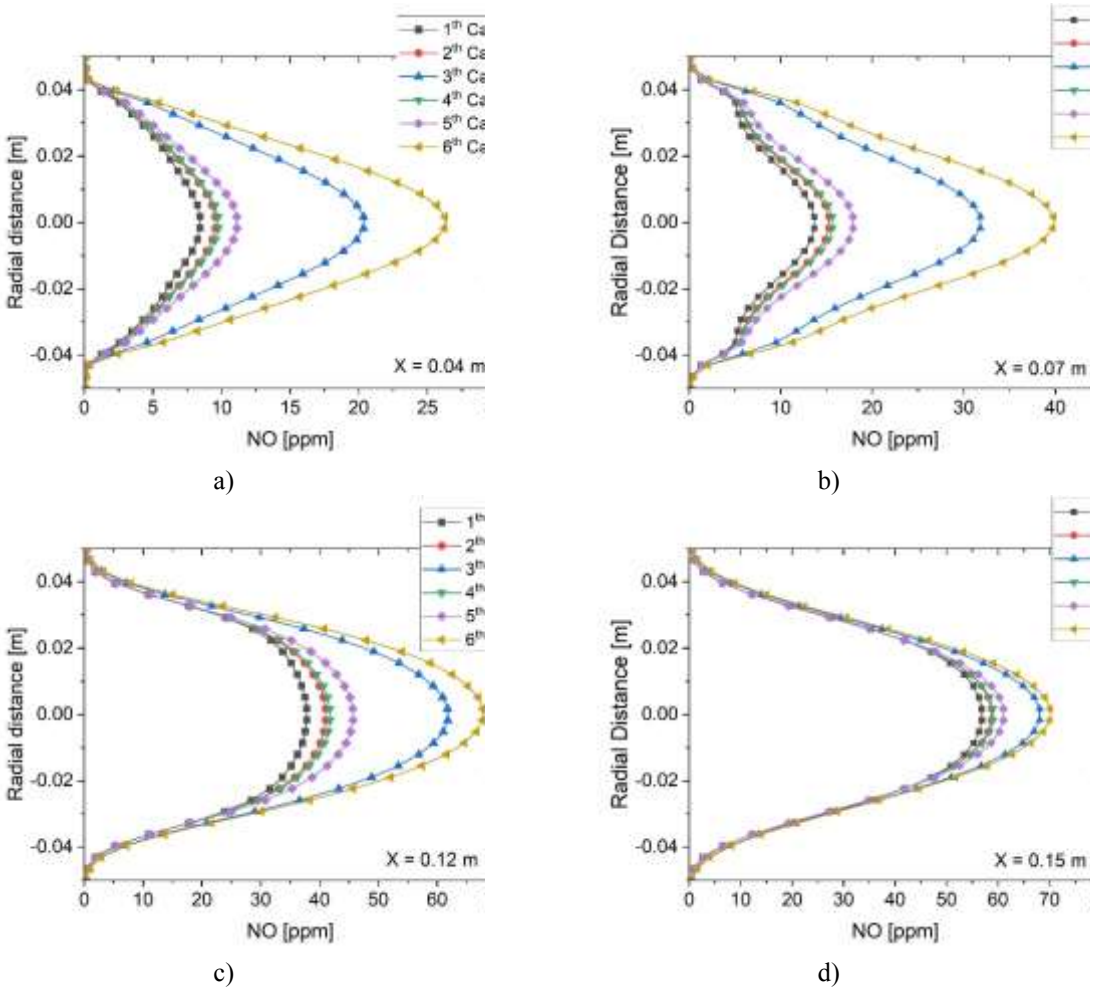

Figure 6 – *NO distribution in various location of the combustor for various cases*

Fig. 7 c. (CO distribution at X = 0.12 m): In every case, CO levels have decreased noticeably by this point. The CO mass percent in the first case is 0.062, and the lowest value is 0.03 in the sixth case. The nearly full combustion that is taking place in the chamber at this moment is reflected in the rapid decrease in CO since the flame has reached steady, high temperatures, thoroughly oxidizing the fuel. The higher temperature and improved fuel-air mixing in the latter situations correlate with the decreased CO production.

Fig. 7 d. (CO distribution at X = 0.15 m): At this final location, CO concentrations continue to decrease, with the sixth case exhibiting the lowest mass fraction of 0.016, and the first case showing a higher value of 0.037. By this moment, the combustion process is essentially complete, and CO levels are at their lowest. The little CO formation across all scenarios implies efficient combustion and the complete oxidation of carbon to CO2. The lower CO levels in the third and sixth cases imply that the greater droplet velocities lead to better mixing and combustion efficiency, minimizing incomplete combustion and consequently CO generation.

Droplet penetration and its impact on combustion dynamics and emissions

In this study, droplet penetration behavior, as illustrated in Fig. 8 a to f for the first through sixth cases, is crucial in defining combustion parameters such as evaporation rates and flame stability. In the first example, droplet penetration is limited, which means that the droplets evaporate quickly after entering the combustion chamber. This quick evaporation causes a more limited and focused combustion process, resulting in lower temperatures, a smaller flame front, and less NOx generation, as seen in the temperature and NO distribution figures. In comparison, the second and fourth cases show modest droplet evaporation and penetration. In these circumstances, the droplets go deeper into the combustion chamber before evaporating, allowing for a more evenly dispersed combustion process. This results in a more balanced temperature distribution and moderate NOx generation. The droplets travel a greater distance than in the first scenario, but they remain inside the core of the flame zone, allowing for successful burning without considerable contact with the combustor walls.

The third, fifth, and sixth cases exhibit maximal droplet penetration and evaporation, with droplets going the greatest distance before entirely evaporating. In certain circumstances, the droplets approach or even strike the combustor internal wall surfaces, resulting in concerns such as wall film development or lower combustion efficiency near the walls. This increased travel distance results in a longer flame front, which leads to higher

temperatures and greater NOx generation, as seen by the higher NO and temperature distribution. Furthermore, in certain cases, contact with the combustor walls might cause localized hotspots and greater emission levels, notably of CO, owing to incomplete combustion along the walls.

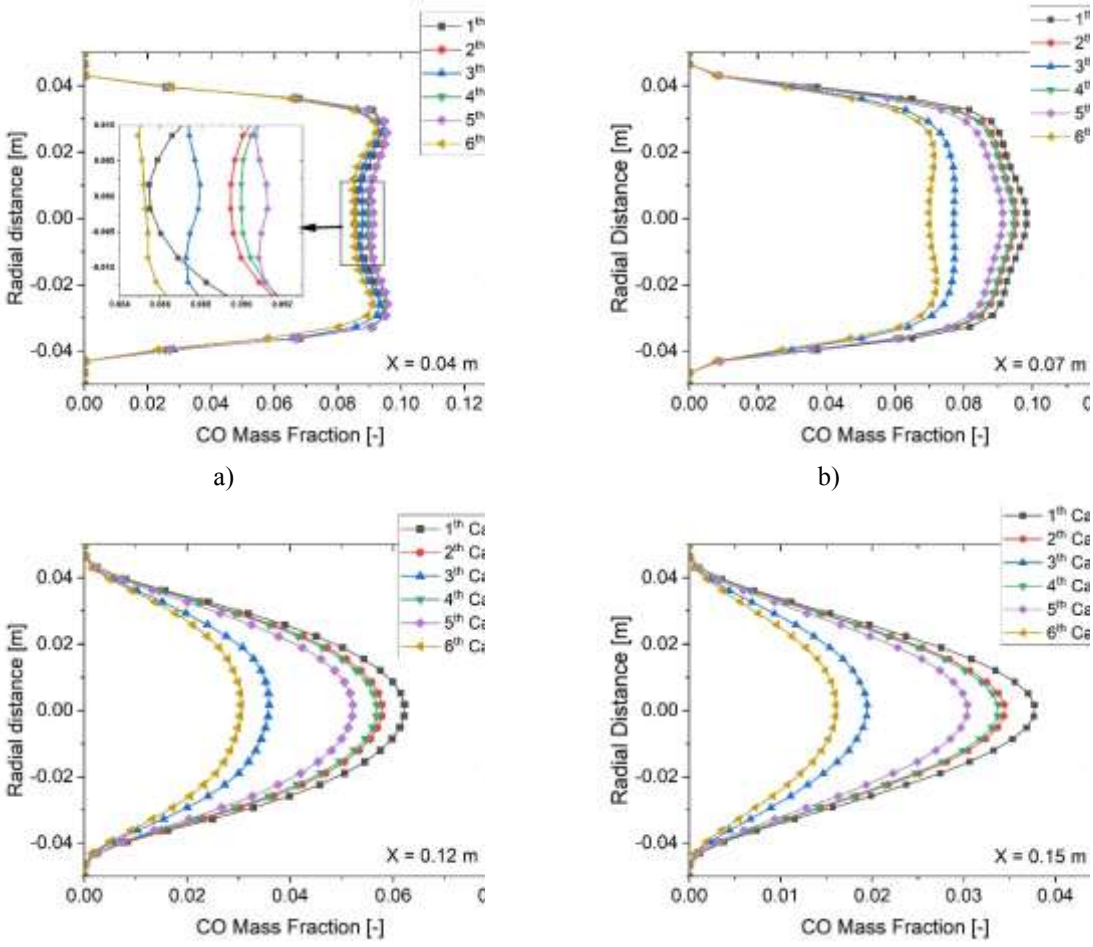

Figure 7 – *CO distribution in various location of the combustor for various cases*

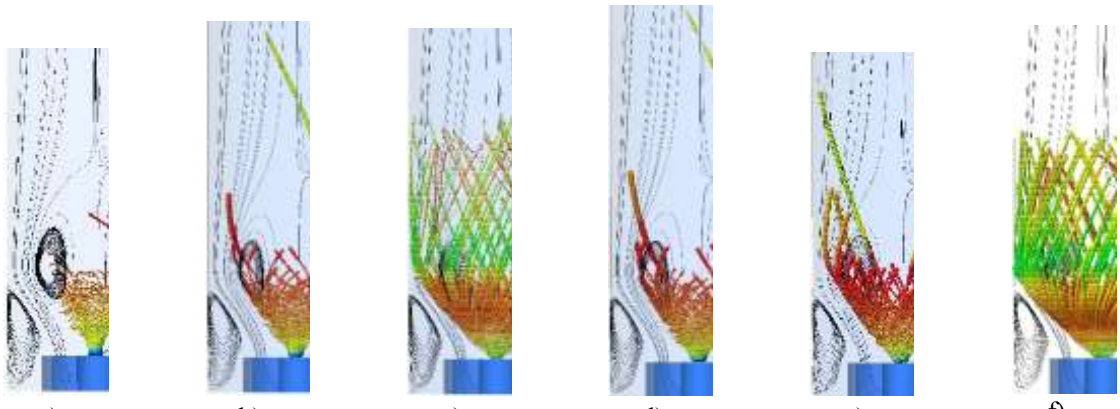

a) b) c) d) e) f)

Figure 8 – *Droplet penetration in to combustor for various cases;*
a) First case b) Second case c) Third case d) Fourth case e) Fifth case f) Sixth case

The change in droplet penetration across all cases demonstrates how droplet behavior directly effects combustion dynamics, flame structure, and emission production in the combustion chamber. The combustion process may be optimized and undesirable emissions like NOx and CO reduced by regulating droplet injection parameters such as velocity and evaporation characteristics.

Investigation of the Temperature, NO and CO formation contour for the first and sixth studied cases

Figures 9a and 9b present contour plots illustrating the temperature spread in the center plane of the combustors for the first and sixth scenarios, respectively In Figure 9a, the situation shows a lower temperature distribution around the fuel injection center and the central recirculation zone (CRZ). This indicates that in first case there is fuel evaporation and combustion due to reduced penetration and evaporation resulting in diminished heat release in these specific regions.

In comparison to Fig. 9b, the sixth situation depicted an uptick in temperature in these areas. The temperature rise could be linked to penetration that allows for a greater amount of fuel to reach the core and CRZ. This results in a combustion process and higher heat output. The differences in temperature spread between the two scenarios suggest that greater radial and tangential speeds in the scenario enhance evaporation and combustion strength, leading to a more effective energy release.

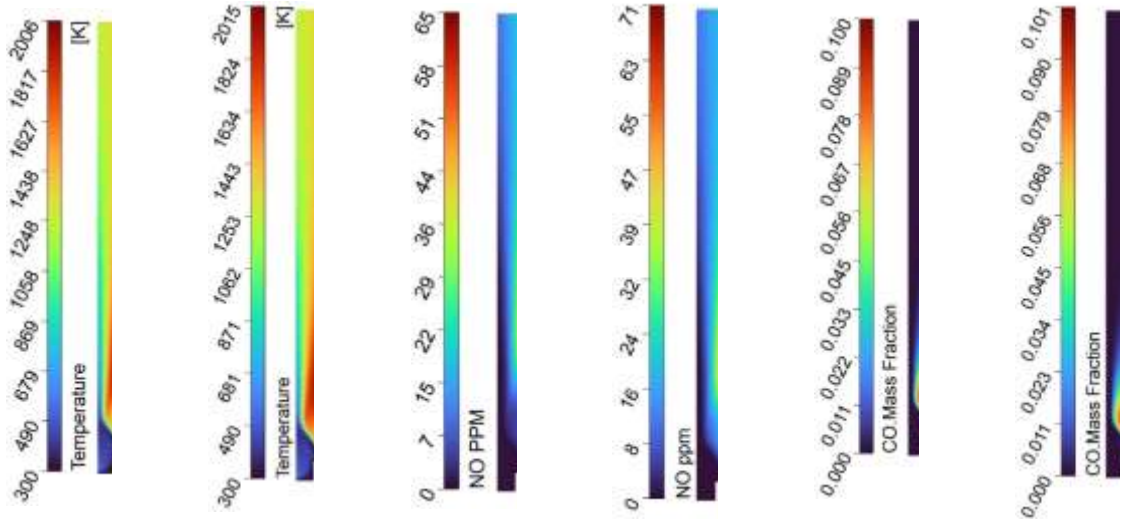

a) b) c) d) e) f)

Figure 9 – *The contour plots of the first and sixth cases; a) Temperature distribution in the first case b) Temperature distribution in the sixth case c) NO distribution in the first case d) NO distribution in the sixth case e) CO distribution in the first case f) CO distribution in the sixth case*

The NO distribution for the first scenario in Fig. 9c shows comparatively lower NO concentrations in the vicinity of the combustor's center plane. This reduced production of NO is consistent with the temperature distribution seen in Fig. 9a, where there is a noticeable decrease in temperature near the fuel injection center and the central recirculation zone (CRZ). Lower temperatures, which restrict the thermal NOx generation process, are thought to be the cause of the first case's decreased NO formations. On the other hand, the NO distribution for the sixth example, where the NO concentrations are noticeably larger than those of the first case, is depicted in Fig. 9d. The higher temperatures shown in Fig. 9b are correlated with this increase in NO production. The sixth case's greater temperatures promote the thermal NOx generation, which raises NO concentrations in the same regions as the temperature. The close correlation between temperature and NO production is highlighted by this comparison. As demonstrated in the sixth example, higher temperatures cause more NO to develop, but lower temperatures cause less NO to be released, as demonstrated in the first example.

The CO distribution contour plots for the first and sixth cases are displayed in Figs. 9e and 9f. The contour plot in Fig. 9e, which shows the CO distribution for the first scenario, shows lower CO concentrations in the area surrounding the combustor's center plane. This outcome is consistent with the reduced NO levels in Fig. 9c and the lower temperatures seen in Fig. 9a. In the first case, where the lower temperature and shorter primary combustion zone lead to less CO formation, the lower CO levels point more thorough combustion and effective oxidation processes. besides that, Fig. 9f displays the CO distribution for the sixth scenario, wherein elevated NO levels, as illustrated in Fig. 9d, and higher CO concentrations are visible in the same regions where the temperature is higher, as indicated in Fig. 9b. In areas with higher temperatures and longer droplet penetration, incomplete combustion and reduced oxidation efficiency can be blamed for the increased CO formation in the sixth example. This shows that although greater temperatures cause more NO to develop, they also raise CO levels because of less complete combustion in those areas. This CO distribution analysis demonstrates how temperature and combustion efficiency interact. If the combustion process is not optimized for complete oxidation, greater temperatures can increase CO emissions in addition to NO generation. On the other hand, as the first example illustrates, lower temperatures and shorter droplet penetration lead to less CO production, which denotes more thorough burning.

Conclusion

This paper investigates how temperature distribution within a gas turbine combustor and NOx and CO emissions are affected by changing the radial and tangential injection velocities of kerosene droplets. The study analyzes six different scenarios with varying injection velocity components using CFD simulations with ANSYS CFX with the goal of comprehending how these factors affect flame stability, heat distribution, and the formation of harmful emissions.

The main conclusions show that injected kerosene droplets with higher radial and tangential velocities greatly improve fuel-air mixing and, consequently, increase combustion efficiency. Higher core temperatures within the combustion zone are indicative of a more stable and intense flame produced by this improved mixing. Temperatures up to 1960K were reached in situations with higher droplet velocities, which encouraged more complete combustion and a more even temperature distribution throughout the combustor.

It was discovered that NOx emissions, especially thermal NOx, were highly temperature-dependent. NOx formation increased along with the droplet velocities, which raised the combustion temperature. The study highlighted the direct relationship between temperature and NOx production by showing that the scenarios with the highest flame temperatures also had the highest NOx concentrations. For example, NOx concentrations at the furthest axial position reached 67 ppm in the highest velocity case.

The relationship between CO emissions and combustion efficiency was inverse. Due to inadequate fuel-air mixing, incomplete combustion produced higher CO emissions in situations with lower droplet velocities. More complete combustion happened as the injection velocities increased, which resulted in a notable drop in CO levels. In the highest velocity case, CO emissions were reduced to a mass fraction of 0.016 at the end of combustion, indicating very effective fuel oxidation.

The accuracy of the simulations is established by validating the CFD model with experimental data, which is a critical component of the study. The results are given more credibility by the comparison with earlier studies, which shows that the CFD model can accurately predict the temperature distribution and formation of NOx in the combustor. The consistency between the experimental and simulated data highlights how reliable the numerical techniques used were.

The study's conclusion demonstrates that kerosene droplet injection velocities can be optimized to have a substantial impact on emission levels and the combustion process. Better mixing and more thorough combustion are facilitated by higher radial and tangential velocities, which lower CO emissions. There is a trade-off between increasing combustion stability and reducing NOx emissions, though, as higher combustion temperatures lead to an increase in NOx formation. Thus, it is essential to strike the ideal droplet velocity balance in order to reduce harmful emissions while preserving stable and effective combustion. This study emphasizes how crucial it is to precisely regulate fuel injection settings in gas turbine engines in order to comply with environmental standards and achieve operational performance objectives.

References:

1. Hajivand, M., & Dolmatov, D. A. (2021). NUMERICAL ANALYSIS OF KEROSENE SPRAY COMBUSTION IN VARIOUS INJECTION PREPARATIONS AND EMISSION BEHAVIOUR ASSESSMENT. Collection of Scientific Publications NUS, 1, 125–141. https://doi.org/10.15589/znp2021.1(484).18

2. Rink, K. K., & Lefebvre, A. H. (1989b). The Influences of Fuel Composition and Spray Characteristics on Nitric Oxide Formation. *Combustion Science and Technology*, *68*(1–3), 1–14. https://doi.org/10.1080/00102208908924066

3. Kankashvar, B., Tabejamaat, S., EidiAttarZade, M., Sadatakhavi, S. M., & Nozari, M. (2021a). Experimental study of the effect of the spray cone angle on the temperature distribution in a can micro-combustor. *Aerospace Science and Technology*, *115*, 106799. https://doi.org/10.1016/j.ast.2021.106799

4. Dafsari, R. A., Lee, H. J., Han, J., & Lee, J. (2019). Evaluation of the atomization characteristics of aviation fuels with different viscosities using a pressure swirl atomizer. *International Journal of Heat and Mass Transfer*, *145*, 118704. https://doi.org/10.1016/j.ijheatmasstransfer.2019.118704

5. Lefebvre, A. H., & McDonell, V. G. (2017b). Atomization and Sprays. In *CRC Press eBooks*. https://doi.org/10.1201/9781315120911

6. Bokhart, A. J. (n.d.). *An Investigation of the Spray Characteristics of Standard and Alternative Fuel Sprays from a Hybrid Airblast Pressure-Swirl Atomizer Operating at Lean Blowout and Chilled Conditions Using Phase Doppler Anemometry.* Purdue e-Pubs. https://docs.lib.purdue.edu/open_access_theses/1255

7. Bishop, K., & Allan, W. (2010b). Effects of Fuel Nozzle Condition on Gas Turbine Combustion Chamber Exit Temperature Distributions. *Volume 2: Combustion, Fuels and Emissions, Parts a and B*. https://doi.org/10.1115/gt2010-23441

8. Lin, B., Wu, Y., Xu, M., & Chen, Z. (2021). Experimental investigation on spark ignition and flame propagation of swirling kerosene spray flames. *Fuel*, *303*, 121254. https://doi.org/10.1016/j.fuel.2021.121254

9. Ghose, P., & Datta, A. (2020). Effect of Inlet Swirl and Turbulence Levels on Combustion Performance in a Model Kerosene Spray Gas Turbine Combustor. In *Lecture notes in mechanical engineering* (pp. 493–504). https://doi.org/10.1007/978-981-15-7831-1_46

10. Alsulami, R., Windell, B., Nates, S., Wang, W., Won, S. H., & Windom, B. (2019). Investigating the role of atomization on flame stability of liquid fuels in an annular spray burner. *Fuel*, *265*, 116945. https://doi.org/10.1016/j.fuel.2019.116945

11. Fathinia, F., Khiadani, M., & Al-Abdeli, Y. M. (2019). Experimental and mathematical investigations of spray angle and droplet sizes of a flash evaporation desalination system. *Powder Technology*, *355*, 542–551. https://doi.org/10.1016/j.powtec.2019.07.081

12. Gong, J., & Fu, W. (2007). The experimental study on the flow characteristics for a swirling gas–liquid spray atomizer. *Applied Thermal Engineering*, *27*(17–18), 2886–2892. https://doi.org/10.1016/j.applthermaleng.2007.04.006

13. Peters, N. (2000b). *Turbulent Combustion*. Cambridge University Press https://doi.org/10.1017/cbo9780511612701

14. Li, Q., Zhang, P., Feng, Y., & Wang, P. (2015). Implementation variations of adiabatic steady PPDF flamelet model in turbulent H2/air non-premixed combustion simulation. *Case Studies in Thermal Engineering*, *6*, 204–211. https://doi.org/10.1016/j.csite.2015.10.001

15. CFX. *ANSYS CFX-Solver Modeling Guide*, ANSYS, Inc., Canonsburg, PA, USA, Release 18.2

16. CFX. *ANSYS CFX-Solver Theory Guide*, ANSYS, Inc., Canonsburg, PA, USA, Release 18.2

17. Pohl, S., Jarczyk, M., Pfitzner, M., & Rogg, B. (2013). Real gas CFD simulations of hydrogen/oxygen supercritical combustion. *Progress in Propulsion Physics*. https://doi.org/10.1051/eucass/201304583

18. Zimmermann, I. (2009). *Modeling and Numerical Simulation of Partially Premixed Flames* [Universität der Bundeswehr München, Fakultät für Luft- und Raumfahrttechnik]. http://athene forschung.unibw.de/node?id=86289

19. Golder, S., & Doom, J. J. (2017b). Simulation of an ethylene flame with turbulence, soot and radiation modeling. *55th AIAA Aerospace Sciences Meeting*. https://doi.org/10.2514/6.2017-0540

20. Modest, M. F. (2013b). Radiative Heat Transfer. In *Elsevier eBooks*. https://doi.org/10.1016/c2010-0-65874-3

21. Höglauer, C., Kniesner, B., Knab, O., Schlieben, G., Kirchberger, C., Silvestri, S., & Haidn, O. J. (2015). Modeling and simulation of a GOX/kerosene subscale rocket combustion chamber with film cooling. *CEAS Space Journal*, *7*(4), 419–432. https://doi.org/10.1007/s12567-015-0096-y

22. Strokach, E. A., Borovik, I. N., Bazarov, V. G., & Haidn, O. J. (2020). Numerical study of operational processes in a GOx-kerosene rocket engine with liquid film cooling. *Propulsion and Power Research*, *9*(2), 132–141. https://doi.org/10.1016/j.jppr.2020.04.004

23. Ghose, P., Datta, A., & Mukhopadhyay, A. (2015). Effect of Prediffuser Angle on the Static Pressure Recovery in Flow Through Casing-Liner Annulus of a Gas Turbine Combustor at Various Swirl Levels. *Journal of Thermal Science and Engineering Applications*, *8*(1). https://doi.org/10.1115/1.4030734

24. Ranz, W. E. ., & Marshall, W. R (1952). Evaporation from drops: Part II. *Chemical Engineering Progress*, *48*, 173–180. http://ci.nii.ac.jp/naid/10020503031

25. Warnatz, J., Maas, U., & Dibble, R. (2006). *Combustion: Physical and Chemical Fundamentals, Modeling and Simulation, Experiments, Pollutant Formation*. https://doi.org/10.1007/978-3-540-45363-5

26. Jiang, B., Liang, H., Huang, G., & Li, X. (2006). Study on NOx Formation in CH4/Air Jet Combustion. *Chinese Journal of Chemical Engineering*, *14*(6), 723–728. https://doi.org/10.1016/s1004-9541(07)60002-0

27. Yang, X., He, Z., Qiu, P., Dong, S., & Tan, H. (2019). Numerical investigations on combustion and emission characteristics of a novel elliptical jet-stabilized model combustor. *Energy*, *170*, 1082–1097. https://doi.org/10.1016/j.energy.2018.12.189

28. Bauer, H. J., Eigenmann, L., Scherrer, B., & Wittig, S. (1995). Local Measurements in a Three Dimensional Jet-Stabilized Model Combustor. *Volume 3: Coal, Biomass and Alternative Fuels; Combustion and Fuels; Oil and Gas Applications; Cycle Innovations*. https://doi.org/10.1115/95-gt-071

29. Kurreck, M., Willmann, M., & Wittig, S. (1998). Prediction of the Three-Dimensional Reacting Two-Phase Flow Within a Jet-Stabilized Combustor. *Journal of Engineering for Gas Turbines and Power*, *120*(1), 77–83. https://doi.org/10.1115/1.2818090

30. Bazdidi-Tehrani, F., & Zeinivand, H. (2010). Presumed PDF modeling of reactive two-phase flow in a three dimensional jet-stabilized model combustor. *Energy Conversion and Management*, *51*(1), 225–234. https://doi.org/10.1016/j.enconman.2009.09.020

31. Zeinivand, H., & Bazdidi-Tehrani, F. (2012). Influence of stabilizer jets on combustion characteristics and NOx emission in a jet-stabilized combustor. *Applied Energy*, *92*, 348–360. https://doi.org/10.1016/j.apenergy.2011.11.033

32. Bazdidi-Tehrani, F., & Teymoori, A. (2022). Optimization of a gas turbine model combustor due to variations in geometrical characteristics of stabilizing air jets. *Applied Thermal Engineering*, *217*, 119206. https://doi.org/10.1016/j.applthermaleng.2022.119206

33. Alemi, E., & Zargarabadi, M. R. (2017). Effects of jet characteristics on NO formation in a jet-stabilized combustor. *International Journal of Thermal Sciences*, *112*, 55–67. https://doi.org/10.1016/j.ijthermalsci.2016.10.001

34. Ghose, P., Patra, J., Datta, A., & Mukhopadhyay, A. (2016). Prediction of soot and thermal radiation in a model gas turbine combustor burning kerosene fuel spray at different swirl levels. *Combustion Theory and Modelling*, 1–29. https://doi.org/10.1080/13647830.2016.1147607

35. Ghose, P., Patra, J., Datta, A., & Mukhopadhyay, A. (2014). Effect of air flow distribution on soot formation and radiative heat transfer in a model liquid fuel spray combustor firing kerosene. *International Journal of Heat and Mass Transfer*, *74*, 143–155. https://doi.org/10.1016/j.ijheatmasstransfer.2014.03.001

М. Хаджівand[1], аспірант; ORCID 0000-0002-9990-9761
Д. Долматов[1], д-р техн.наук; ORCID 0000-0002-7268-1509
[1]Національний аерокосмічний університету ім. Н.Є. Жуковського «ХАІ»

ВПЛИВ ІН'ЄКЦІЇ КРАПЕЛЬ РІДКОГО КЕРОСИНУ ПРИ РІЗНИХ РАДІАЛЬНИХ ТА ТАНГЕНЦІЙНИХ ШВИДКОСТЯХ НА УТВОРЕННЯ NOX, CO ТА РОЗПОДІЛ ТЕМПЕРАТУРИ

У цьому дослідженні представлено числовий аналіз і CFD-моделювання згоряння рідкого керосину шляхом варіювання радіальних і тангенціальних складових швидкості крапель керосину, інжектованих через форсунку в реальний камеру згоряння. Краплі розглядаються через розподіл розмірів частинок за Розіном-Раммлером з використанням моделі розпилення Ейлера-Лагранжа. Основною метою цього дослідження є оцінка процесів утворення викидів, таких як NO і CO, а також коливань розподілу температури в зоні первинного згоряння під час процесу горіння та випаровування крапель. Для моделювання горіння випареного керосину було використано модель Flamelet, яка дозволяє детально описати кінетичну схему хімічних реакцій між (JetA-C10H22) і повітрям, інтегровану в ANSYS CFX, включаючи термічне та швидке утворення NO. Було застосовано стандартну модель турбулентності k-є з покращеним описом стінок і моделлю випромінювання P1. Верифікація та валідація результатів аналізу були розглянуті в цьому дослідженні, де результати, такі як розподіл температури та утворення NO на різних радіальних відстанях камери згоряння, порівнювалися з реальними експериментальними даними. Результати показали, що поведінка крапель, зумовлена швидкостями інжекції, значно впливає на процес згоряння, включаючи розподіл температури, утворення NOx та викиди CO, особливо в зоні первинного згоряння.

Ключові слова: *CFD, згоряння, розпилення, викиди, спрей, випаровування крапель, флеймлет.*

Надійшла: 25.09.2024
Received: 25.09.2024